Diffusion Priors for Variational Likelihood Estimation and Image Denoising

Jun Cheng, Shan Tan*
School of Artificial Intelligence and Automation,
Huazhong University of Science and Technology
jcheng24@hust.edu.cn, shantan@hust.edu.cn

Abstract

Real-world noise removal is crucial in low-level computer vision. Due to the remarkable generation capabilities of diffusion models, recent attention has shifted towards leveraging diffusion priors for image restoration tasks. However, existing diffusion priors-based methods either consider simple noise types or rely on approximate posterior estimation, limiting their effectiveness in addressing structured and signal-dependent noise commonly found in real-world images. In this paper, we build upon diffusion priors and propose adaptive likelihood estimation and MAP inference during the reverse diffusion process to tackle real-world noise. We introduce an independent, non-identically distributed likelihood combined with the noise precision (inverse variance) prior and dynamically infer the precision posterior using variational Bayes during the generation process. Meanwhile, we rectify the estimated noise variance through local Gaussian convolution. The final denoised image is obtained by propagating intermediate MAP solutions that balance the updated likelihood and diffusion prior. Additionally, we explore the local diffusion prior inherent in low-resolution diffusion models, enabling direct handling of high-resolution noisy images. Extensive experiments and analyses on diverse real-world datasets demonstrate the effectiveness of our method. Code is available at https://github.com/HUST-Tan/DiffusionVI.

1 Introduction

Real-world imaging modalities, such as photography and biomedical imaging, frequently encounter complex image noise that is both signal-dependent and spatially correlated [23, 35]. Removing such noise is critical for subsequent image analysis and understanding. Existing deep learning-based image denoising methods rely on either large amounts of paired images for supervised training [50, 48, 49, 25] or noisy images for self-supervised training [31, 23, 46, 33]. However, collecting massive amounts of data is expensive and time-consuming in real-world scenarios. Therefore, designing effective and data-efficient real-world denoising methods is of significant practical importance.

Incorporating image priors and the likelihood, and conducting the corresponding posterior inference (e.g., maximum-a-posteriori (MAP) estimation and mean estimation), is a classical and data-efficient approach to image restoration [26, 18]. Nowadays, deep generative models such as VAE, GAN, and Normalizing-flow have shown the capacity to capture and model complex image statistics, surpassing traditional analytical image priors [32]. Recent diffusion models have demonstrated state-of-the-art image generation capabilities [14, 37] and have been incorporated into various image restoration tasks as powerful image priors [19, 12, 5].

*Corresponding Author

38th Conference on Neural Information Processing Systems (NeurIPS 2024).

The essence of applying diffusion priors to address image denoising lies in accurately integrating the degraded image into the generation process of pre-trained diffusion models, underscoring the importance of the likelihood function. Unlike Gaussian white noise, real-world image noise is intricate and challenging to model precisely and analytically [17, 21]. Many existing methods based on diffusion priors solely account for $i.i.d.$ Gaussian noise [19, 5, 43, 10], making them ineffective for real-world noise removal. On the other hand, some approaches targeting complex and non-linear degradations employ *hard* data-consistency strategies and approximate posterior inference during the generation process [12, 45, 8], yielding unsatisfactory real-world denoising outcomes due to their coarse likelihood modeling. Although a structured and heteroscedastic Gaussian likelihood function can well approximate real-world noise, such a model is computationally expensive due to the large covariance matrix and also impractical due to the unknown noise variance.

To tackle these challenges, this paper integrates variational Bayes and presents adaptive likelihood estimation and MAP inference during the generation process of diffusion priors to handle real-world noise. We introduce an independent, non-identically distributed ($i.ni.d.$) likelihood combined with a precision prior to model real-world noise. Such a choice allows modeling the spatially variant feature of noise and meanwhile avoids modeling covariance, trading off the accuracy for practical feasibility. Based on variational Bayes, the $i.ni.d.$ precision posterior at each step in the reverse process is subsequently inferred, which adaptively refines the likelihood function and aligns with the real-world noise model. Additionally, we introduce local Gaussian convolution to rectify the estimated noise variance, compensating for the lack of spatial correlation in the $i.ni.d.$ likelihood function. By adaptively updating the likelihood at each reverse diffusion step, the final denoised result is achieved by progressively propagating the intermediate MAP solutions that strike the best balance between the noisy image and diffusion prior.

Furthermore, real-world images exhibit diverse resolutions, often differing from those of pre-trained diffusion models. Existing methods utilize patch-based [12] or resize-based [19] operations, which are laborious and may impact low-level details. We observe that diffusion models pre-trained with low-resolution (LR) images tend to yield local diffusion priors effective for image restoration, enabling the direct treatment of high-resolution (HR) noisy images. The main contributions of this paper are summarized as follows:

- We propose adaptive likelihood estimation and MAP inference based on diffusion priors and variational Bayes to address real-world complex noise.
- We explore the local prior exhibited by diffusion models pre-trained with LR images.
- Our method outperforms other unsurpervised denoising methods as well as diffusion priors-based methods on diverse real-world image denoising datasets.

2 Related Works

Deep Learning-based Image Denoising. By harnessing modern deep architectures and large-scale paired training datasets, supervised learning-based denoising methods such as VDN [48], Restormer [49], and GRL [25] have significantly enhanced in-distribution denoising performance. However, their reliance on extensive paired data poses challenges for real-world applications, prompting the exploration of self-supervised denoising approaches. These include Blind spot (BS)-based methods (e.g., SSDN [22], Noise2Self [3], Nei2Nei [16], and B2U [44]), resampling-based methods (e.g., Nr2N [29] and R2R [34]), and regularization-based methods (e.g., Noise2Score [20] and Stein [38]). However, these methods assume spatially independent or analytical noise, which deviates from the structured and complex real-world noise. Recent advancements, such as AP-BSN [23] and LG-BPN [46], have integrated Pixel-shuffle and masked convolution into BS networks to address real-world noise. Other approaches have leveraged disentangled representation learning [11, 31, 6]. Nonetheless, these methods often require large quantities of noisy images and lack data efficiency. Several single image-based deep learning methods (e.g., DIP [42], Self2Self [36], ZS-N2N [27], and ScoreDVI [7]) have been proposed, but their performance in real-world denoising scenarios remains suboptimal, underscoring the need for more effective approaches.

Diffusion Priors for Image Restoration. Diffusion models have exhibited remarkable image generation capabilities [14, 40, 37] and have been integrated into inverse problems as diffusion priors to address various image restoration tasks in an unsupervised manner [24]. Existing methods based on diffusion priors can be broadly categorized into two aspects: linear inverse problem-solving based on exact degradation models (e.g., DDRM [19], DDNM [43], MCGDiff [5], and FPS [10]), and nonlinear inverse problem-solving based on approximate posterior inference (e.g., DPS [8], GDP [12], and DR2 [45]). In the former, these methods typically assume analytical noise, such as additive white Gaussian noise, overlooking real-world noise that is signal-dependent and spatially correlated. Given the difficulty in precisely modeling and estimating real-world noise, these methods often prove ineffective in handling such noise.

In the latter, *hard* data-consistency terms are introduced to replace accurate likelihood modeling, and approximate posterior inference is conducted during the inverse diffusion process to address complex degradations. However, due to the absence of explicit constraints from likelihood functions, these methods heavily rely on proper hyperparameters (e.g., guidance scales in GDP [12], step size in DPS [8], or downsampling factors in DR2 [45]), leading to significant reconstruction errors. Diverging from these methods, we refrain from specifying the accurate noise model but introduce the noise precision prior and dynamically estimate its posterior using variational Bayes in the reverse diffusion process, enabling adaptive estimation of likelihood functions and better posterior inference.

3 Methods

3.1 Preliminary

The Diffusion model is a class of generative models used to model the distribution $q(x_0)$. Its forward process is a Markov chain with fixed Gaussian transition and length T, which gradually corrupts the data x_0 by adding Gaussian noise according to a pre-defined variance schedule $\eta_1, \cdots, \eta_T$:

$$q(x_{1:T}|x_0) = \prod_{t=1}^{T} q(x_t|x_{t-1}), q(x_t|x_{t-1}) = \mathcal{N}(x_{t-1}; \sqrt{1-\eta_t}x_{t-1}, \eta_t I) \tag{1}$$

A nice property of the forward process is that sample x_t at any step t can be obtained from x_0 in a closed-form manner:

$$q(x_t|x_0) = \mathcal{N}(x_t; \sqrt{\bar{a}_t}x_0, (1-\bar{a}_t)I) \rightarrow x_t = \sqrt{\bar{a}_t}x_0 + \sqrt{1-\bar{a}_t}\epsilon \tag{2}$$

where $a_t = 1 - \eta_t, \bar{a}_t = \prod_{s=1}^{t} a_s, \epsilon \sim \mathcal{N}(0, I)$.

In the reverse process, the diffusion model progressively recovers data from noise distribution $p(x_T)$, which is again a Markov chain with learned Gaussian transition:

$$p(x_{0:T}) = p(x_T) \prod_{t=1}^{T} p(x_{t-1}|x_t), p(x_{t-1}|x_t) = \mathcal{N}(\mu_\theta(x_t, t), \sigma_t^2 I) \tag{3}$$

where σ_t^2 is a constant relating to η_t and can be pre-computed. And $\mu_\theta(x_t, t)$ is usually parameterized by a DNN $\epsilon_\theta(x_t, t)$:

$$\mu_\theta(x_t, t) = \frac{1}{\sqrt{a_t}} \left(x_t - \frac{\beta_t}{\sqrt{1-\bar{a}_t}} \right) \epsilon_\theta(x_t, t) \tag{4}$$

3.2 Naive Image Denoising

Consider the image formation process $y_0 = f(x_0, n)$ in the real-world scenario, where n is the raw noise, f is the transformation function, $y_0 \in \mathbb{R}^N$ and $x_0 \in \mathbb{R}^N$ (N is the total pixel number) are the observed noisy image and original clean image, respectively. Noise in y_0 generally exhibits signal-dependent and spatially-correlated characteristics, e.g., sRGB noise [23], due to the Poisson nature of photons and compound transformation in f. Suppose there are no non-linear parts in f, the image formation process can be simplified as $y_0 = x_0 + n_0(x_0)$ with corr$(n_0^i, n_0^j) > 0$, where n_0 is the image noise related to the signal x_0; corr(i, j) represents the correlation coefficient between two neighboring elements i and j.

Real-world image denoising task is to recover clean and high-quality x_0 from noisy y_0, which turns into solving the posterior $p(x_0|y_0)$ in Bayesian statistics. As the pre-trained diffusion model possesses superior image priors, it is natural to inject the observed information y_0 into its reverse diffusion (or generation) process defined in Eq. (3) to achieve the conditional inference of $x_{0:T}$ given y_0, i.e., $p(x_{0:T}|y_0)$. Due to that y_0 and intermediate x_t exhibit large distribution gaps (as they have different noise types and strength) and it is also difficult to directly model $p(y_0|x_t)$ [8], we hence follow [39, 45] and re-corrupt y_0 using Eq. (2) in each step t to obtain y_t, which serves as intermediate conditions. Such choice results in the target conditional distribution:

$$p(x_{0:T}|y_0) \to p(x_T)\prod_{t=1}^{T} p(x_{t-1}|x_t, y_{t-1}) \propto p(x_T)\prod_{t=1}^{T} p(x_{t-1}|x_t)p(y_{t-1}|x_{t-1}) \tag{5}$$

where $y_t = \sqrt{\overline{a}_t}y_0 + \sqrt{1-\overline{a}_t}\epsilon$, and $p(x_T|y_T) \approx p(x_T)$ as x_T and y_T are approximated independent normal distributions.

Structured and heteroscedastic Gaussian likelihood model. The right-hand side of Eq. (5) explicitly involves the prior $p(x_{t-1}|x_t)$ and likelihood $p(y_{t-1}|x_{t-1})$ at each step t. The prior $p(x_{t-1}|x_t)$ has been available from the pre-trained diffusion model in Eq. (3), necessitating the modeling of $p(y_{t-1}|x_{t-1})$. As discussed above, in principle we can assume that y_0 follows the structured and heteroscedastic Gaussian distribution $\mathcal{N}(x_0, \Sigma(x_0))$, where Σ is the *non-diagonal* covariance matrix with variances related to signal x_0, which allows modeling the signal-dependent and spatially-correlated properties of real-world noise. As a result, we derive that

$$y_{t-1} = \sqrt{\overline{\alpha}_{t-1}}\,(x_0 + A\epsilon_2) + \sqrt{1-\overline{\alpha}_{t-1}}\epsilon = x_{t-1} + \sqrt{\overline{\alpha}_{t-1}}A\epsilon_2, AA^T = \Sigma(x_0), \epsilon_2 \sim \mathcal{N}(0, I) \tag{6}$$

which indicates that $p(y_{t-1}|x_{t-1}) = \mathcal{N}(y_{t-1}; x_{t-1}, \Sigma(x_{t-1}))$ with $\Sigma(x_{t-1}) = \overline{\alpha}_{t-1}\Sigma(x_0)$. See detailed derivation in the Appendix A.1.

As the prior $p(x_{t-1}|x_t)$ in Eq. (3) and likelihood $p(y_{t-1}|x_{t-1})$ in Eq. (6) both have Gaussian forms, the posterior distribution in Eq. (5) is theoretically computable. Nevertheless, we note that the above formulation presents several practical challenges. First, specifying an accurate $\Sigma(x_0)$ for y_0 is *difficult*, which involves the estimation of noise variance and the noise correlation between neighboring pixels. These estimations are hard to achieve based on a single y_0 and are open research problems [17, 21]. In addition, the posterior inference with non-diagonal covariance matrix Σ is both memory-demanding and computationally expensive. These challenges prevent the direct application of the structured heteroscedastic Gaussian likelihood.

3.3 Variational Denoising with Adaptive Likelihood Estimation

To deal with these difficulties, we consider $p(y_0|x_0) = \mathcal{N}(x_0, \text{diag}(\phi_0)^{-1})$, which has diagonal precision matrix diag(ϕ_0) (i.e., the inverse of the covariance matrix, $\phi_0 \in \mathbb{R}^N$). Such diagonal Gaussian likelihood allows modeling the spatially variant feature of real-world noise but ignores the noise correlation at this stage. Based on Eq. (6), $p(y_{t-1}|x_{t-1})$ then becomes:

$$p(y_{t-1}|x_{t-1}, \phi_{t-1}) = \mathcal{N}(y_{t-1}; x_{t-1}, \text{diag}(\phi_{t-1})^{-1}), \phi_{t-1} = \frac{\phi_0}{\overline{\alpha}_{t-1}} \tag{7}$$

Hyperprior for precision ϕ_t. Instead of specifying an accurate ϕ_0, which is again difficult, we introduce the independent Gamma hyperprior $p(\phi_0) = \prod_{i=1}^{N} \text{Gamma}(\phi_0^i; \alpha, \beta)$ for ϕ_0 (α and β are scalars), which serves as the *rough* precision prior for noise in y_0. Meanwhile, based on Eq. (7), it is straightforward that ϕ_{t-1} follows

$$p(\phi_{t-1}) = \prod_{i=1}^{N} \text{Gamma}(\phi_{t-1}^i; \alpha_{t-1}, \beta_{t-1}), \text{with } \alpha_{t-1} = \alpha, \beta_{t-1} = \beta\overline{\alpha}_{t-1} \tag{8}$$

Because $p(\phi_{t-1})$ merely provides initial gauss about the noise precision (also variance) at each step t, we then expect to find the corresponding precision posterior $p(\phi_{t-1}|x_{t-1}, y_{t-1})$, which is more accurate and allows a better likelihood function $p(y_{t-1}|x_{t-1})$. As posterior ϕ_{t-1} depends on x_{t-1}, we have to simuteniously infer them together, i.e., the following joint distribution:

$$p(x_{t-1}, \phi_{t-1}|x_t, y_{t-1}) = \frac{p(y_{t-1}|x_{t-1}, \phi_{t-1})^{\frac{1}{\gamma}} p(\phi_{t-1}) p(x_{t-1}|x_t)}{p(y_{t-1}|x_t)} \tag{9}$$

where $\gamma \leq 1$ is the temperature parameter, which is typically utilized in variational inference to scale the likelihood function [2].

Variational inference of precision posterior. As $p(x_{t-1}, \phi_{t-1}|x_t, y_{t-1})$ in Eq. (9) is a non-trivial distribution, we hence choose a trivial and factorized variational distribution $g(x_{t-1}, \phi_{t-1}) = g(x_{t-1})g(\phi_{t-1})$ to approximate the true posterior $p(x_{t-1}, \phi_{t-1}|x_t, y_{t-1})$, under the KL-divergence distance. Following the mean-field variational Bayes presented in [4], the optimal $g(x_{t-1})g(\phi_{t-1})$ can be solved by cycling through x_{t-1} and ϕ_{t-1} and replacing each in turn with a revised estimate of $g(x_{t-1})$ and $g(\phi_{t-1})$. Specifically, we derive the following alternate update scheme for finding the optimal $g(\phi_{t-1})$:

1. Update $g(x_{t-1})$. Given $g(\phi_{t-1})$, the optimal $g^*(x_{t-1})$ is provided by

$$\log g^*(x_{t-1}) = \mathrm{E}_{\phi_{t-1}} \log p(y_{t-1}|x_{t-1}, \phi_{t-1})^{\frac{1}{\gamma}} p(x_{t-1}|x_t)p(\phi_{t-1}) \tag{10}$$

which corresponds to

$$g^*(x_{t-1}) = \mathcal{N}(x_{t-1}; \hat{\mu}_{t-1}, \hat{\sigma}^2_{t-1}) \tag{11}$$

with mean $\hat{\mu}_{t-1}$ and variance $\hat{\sigma}^2_{t-1}$ as

$$\hat{\mu}_{t-1} = \frac{\sigma_t^2 \mathrm{E}(\phi_{t-1}) \odot y_{t-1} + \mu_\theta(x_t, t)\gamma}{\mathrm{E}(\phi_{t-1})\sigma_t^2 + \gamma}, \hat{\sigma}^2_{t-1} = \mathrm{diag}\left(\frac{\gamma\sigma_t^2}{\mathrm{E}(\phi_{t-1})\sigma_t^2 + \gamma}\right) \tag{12}$$

where $\odot$ denotes element-wise multiplication; $\mathrm{E}(\phi_{t-1})$ at step T is initialized as a constant (which is robust to different initializations) and then is updated as $\mathrm{E}(\phi_{t-1}) = \hat{\alpha}_{t-1}/\hat{\beta}_{t-1}$ (see **Update 2**).

2. Update $g(\phi_{t-1})$. Similar to $g(x_{t-1})$, the optimal $g^*(\phi_{t-1})$ given $g(x_{t-1})$ is

$$g^*(\phi_{t-1}) = \prod_{i=1}^{N} \mathrm{Gamma}(\phi^i_{t-1}; \hat{\alpha}^i_{t-1}, \hat{\beta}^i_{t-1}) \tag{13}$$

with shape $\hat{\alpha}_{t-1}$ and rate $\hat{\beta}_{t-1}$ as

$$\hat{\alpha}^i_{t-1} = \alpha_{t-1} + \frac{1}{2\gamma}, \hat{\beta}^i_{t-1} = \beta_{t-1} + \frac{(y^i_{t-1} - \hat{\mu}^i_{t-1})^2 + (\hat{\sigma}^2_{t-1})^i}{2\gamma} \tag{14}$$

The detailed derivation of Eqs. (11) and (13) is given in the Appendix A.2.

MAP estimation with updated likelihood. During the updates, $\hat{\alpha}_{t-1}$ and $\hat{\beta}_{t-1}$ in $g(\phi_{t-1})$ are adptively updated and become signal-dependent as indicated by Eq. (14). Once the cycling converges, we can obtain the approximated posterior distribution $g(\phi_{t-1})$ and the updated likelihood $p(y_{t-1}|x_{t-1}) = \mathrm{E}_{\phi_{t-1}\sim g(\phi_{t-1})} p(y_{t-1}|x_{t-1}, \phi_{t-1})$ at step t. As a result, by maximizing the conditional distribution in Eq. (5) at step t, the optimal x^*_{t-1} that balances the image prior and the observed y_{t-1} can be obtained as follows:

$$\begin{aligned}
x^*_{t-1} &= \mathrm{argmax}\ \log p(y_{t-1}|x_{t-1}) + \log p(x_{t-1}|x_t) \\
&\approx \mathrm{argmax}\ \mathrm{E}_{\phi_{t-1}} \log p(y_{t-1}|x_{t-1}, \phi_{t-1}) + \log p(x_{t-1}|x_t) \\
&= \mathrm{argmax}\ -(x_{t-1} - y_{t-1})^2 \mathrm{E}(\phi_{t-1}) - \frac{(x_{t-1} - \mu_\theta(x_t, t))^2}{\sigma_t^2} \\
&= \hat{\pi}_{t-1} y_{t-1} + (1 - \hat{\pi}_{t-1})\mu_\theta(x_t, t), \text{with } \hat{\pi}_{t-1} = \frac{\sigma_t^2}{\sigma_t^2 + 1/\mathrm{E}(\phi_{t-1})}
\end{aligned} \tag{15}$$

where $\mathrm{E}(\phi_{t-1}) = \hat{\alpha}_{t-1}/\hat{\beta}_{t-1}$ is the expectation of noise precision posterior (and hence $1/\mathrm{E}(\phi_{t-1}) = \hat{\beta}_{t-1}/\hat{\alpha}_{t-1}$ is the estimated noise variance at step t), and $\hat{\pi}_t \in [0, 1]$ suggests that the optimal x^*_{t-1} is the convex combination of y_{t-1} and $\mu_\theta(x_t, t)$. Note that, in the second row of Eq. (15), we utilize the following Jensen's Inequality

$$\log p(y_{t-1}|x_{t-1}) = \log \mathrm{E}_{\phi_{t-1}\sim g(\phi_{t-1})} p(y_{t-1}|x_{t-1}, \phi_{t-1}) \geq \mathrm{E}_{\phi_{t-1}\sim g(\phi_{t-1})} \log p(y_{t-1}|x_{t-1}, \phi_{t-1}) \tag{16}$$

and employ the lower bound of $\log p(y_{t-1}|x_{t-1})$. Optimizing this lower bound generally produces satisfactory solutions, like in variational inference, VAE, and diffusion models.

Rectification of $1/\mathbf{E}(\phi_{t-1})$. By considering the diagonal Gaussian likelihood, the noise correlation between neighboring pixels in y_0 (and y_t) is ignored, which affects the estimation of the precision

Algorithm 1 Difusion priors-based variational image denoising

Input: Pre-trained diffusion model, noisy observation y_0, hyperparameters α, β, temperature γ

$x_T \sim \mathcal{N}(0, I), \mathrm{E}(\phi_T) = \vec{1}$
for $t = T, \cdots, 1$ **do**
    Compute $\mu_\theta(x_t, t)$ based on Eq. (4); Compute y_{t-1} based on Eq. (7)
    Set $\hat{\mu}_{t-1}^{\text{old}} = \vec{0}, \hat{\mu}_{t-1} = \mu_\theta(x_t, t)$
    while $\|\hat{\mu}_{t-1}^{\text{old}} - \hat{\mu}_{t-1}\|_2^2 \geq 1e^{-6}$ **do**
        Update $g(x_{t-1}) = \mathcal{N}(\hat{\mu}_{t-1}, \hat{\sigma}_{t-1}^2)$ using Eq. (12)
        Update $g(\phi_{t-1}) = \prod_{i=1}^{N} \text{Gamma}(\hat{\alpha}_{t-1}^i, \hat{\beta}_{t-1}^i)$ using Eq. (14)
    end while
    Solve optimal x_{t-1} using Eq. (15) or Eq. (17)
end for
return x_0

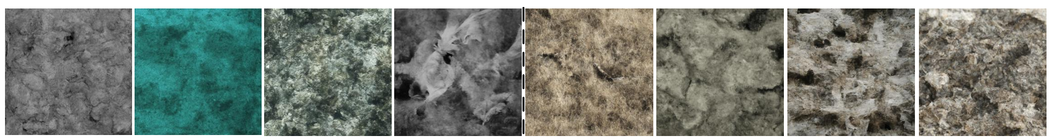

256×256 images sampled from 128×128 diffusion model 512×512 images sampled from 256×256 diffusion model

Figure 1: Unconditional HR images generation from LR diffusion models

posterior and noise variance $1/\mathrm{E}(\phi_{t-1})$. This is apparent as transformations in f (e.g., demosaicking in the ISP pipeline) will cause the local correlation of noise variance (or precision) while elements in $\mathrm{E}(\phi_{t-1})$ are updated independently as shown in Eq. (14). Motivated by the analysis of spatial correlation of real-world noise in [23], we introduce a local 2D convolution with a normalized Gaussian kernel $G(l, s)$ (l is kernel size and s is the scale) to manually rectify $1/\mathrm{E}(\phi_{t-1})$. That is,

$$\overline{1/\mathrm{E}(\phi_{t-1})} = \text{Conv}(1/\mathrm{E}(\phi_{t-1}), G(l, s)), \hat{\pi}_{t-1} = \frac{\sigma_t^2}{\sigma_t^2 + \overline{1/\mathrm{E}(\phi_{t-1})}} \tag{17}$$

By progressively calculating x_{t-1}^* at each step t based on Eqs. (15) and (17), the final denoised result x_0 can be obtained. The whole denoising algorithm is presented in Alg. 1.

3.4 Local Diffusion Priors

The common practice of sampling images from pre-trained diffusion models is to maintain the sampling resolution identical to the training resolution, which produces the best generation performance. In image restoration tasks, however, the resolution of the observed noisy image generally mismatches that of the pre-trained diffusion model. Existing approaches typically use patches [12] or resize operations [19] to address this issue, which is cumbersome and may affect local details.

We observe that when a diffusion model trained with the U-Net architecture on low-resolution (LR) images is employed to sample high-resolution (HR) images, it exhibits local properties. Fig. 1 shows sampled 512×512 and 256×256 images from pre-trained 256×256 [2] and 128×128 [3] diffusion models, respectively, and it is clear that the generated textures mainly focus on local areas. As HR images contain more redundant information, denoising HR images is simpler than denoising their LR counterparts under the same noise level [41]. When the LR diffusion model is used to generate HR samples, there is only a short time window for it to decide the structures of the sampled images [15], thus the generation tends to be local. Similar to traditional TV priors and Markov random fields that focus on designing local image statistics, we note that the local property of LR diffusion models is also effective for image denoising. This allows us to directly adopt the pre-trained LR diffusion prior to denoise HR noisy images without additional operations.

[2] https://openaipublic.blob.core.windows.net/diffusion/jul-2021/256x256_diffusion_uncond.pt
[3] https://openaipublic.blob.core.windows.net/diffusion/jul-2021/128x128_diffusion.pt

Table 1: Selection of β and s for different test datasets.

Datasets	SIDD	FMDD	CC	PolyU	Datasets	SIDD	FMDD	CC	PolyU
β value	0.03	0.025	0.01	0.005	s value	0.6	1.0	1.0	1.0

4 Experiments

4.1 Experimental settings

Datasets. We consider several real-world denoising datasets to evaluate our method, including SIDD [1], PolyU [47], CC [30], and FMDD [51]. SIDD validation, PolyU and CC datasets contain natural sRGB images from smartphones or commercial camera brands, where SIDD consists of 1280 patches with size $3 \times 256 \times 256$, PolyU and CC consist of 100 and 15 natural images with size $3 \times 512 \times 512$, respectively. FMDD contains 48 fluorescence microscopy images with size 512×512.

Implementation Details. We utilize the 256×256 unconditional diffusion model [2] provided by [9] as the diffusion prior throughout our main experiments, regardless of the resolution of input noisy images. The total diffusion steps are 1000 by default, i.e., $t \in [1, \cdots, 1000]$. We choose $\alpha = 1$ and Gaussian kernel size $l = 9$. The hyperparameters β and s for different datasets are summarized in Table 1. Different α/β represent the rough estimation of the prior precision for noises in different datasets, and Gaussian kernel scale s controls the range of local spatial correlation. The temperature γ is set to $1/5$ for all datasets and will be ablated in the sequel. For SIDD dataset, the sizes of $x_{0:T}$ are $3 \times 256 \times 256$. For the remaining datasets, they are $3 \times 512 \times 512$. The denoised results for FMDD are obtained by averaging the channel dimension of x_0 to get one-channel images. All experiments are conducted on Nvidia 2080Ti GPU.

Compared methods. We consider several representative single image-based unsupervised denoising methods, including DIP [42], Self2Self [36], PD-denoising [52], ZS-N2N [27], and ScoreDVI [7]. We also compare against AP-BSN [23], a self-supervised denoising method that can be trained on noisy images of test sets directly. In addition, several diffusion priors-based image restoration methods, including DDRM [19], GDP [12], and DR2 [45], are chosen to denoise real-world images. For these compared methods, we utilize their official source code and report the corresponding performance. Particularly, these diffusion-based methods employ the same diffusion prior [2] as ours. As DDRM can only handle $i.i.d.$ Gaussian noise and requires the noise std σ_{ddrm}, we hence set $\sigma_{\text{ddrm}} = \sqrt{\beta/\alpha}$, i.e., the prior noise std in our method. GDP introduced the hard data-fidelity term $\hat{s}\|\hat{x}_0 - y_0\|_2^2$, where $\hat{x}_0$ is the estimated denoised result at each reverse diffusion step, and $\hat{s}$ is the guidance scale. We tune different $\hat{s}$ for different datasets. DR2 first obtained the intermediate x_{t-1} by adopting a low-pass filter Φ_D and setting $x_{t-1} = \Phi_D y_{t-1} + (1 - \Phi_D)x_{t-1}$ and then conducted inference from step $\tau + 0.25T$ to τ. We set $D = 8$ (Downsampling factor) and $\tau = 100$ for DR2. We evaluate the quantitative denoising quality using PSNR and SSIM metrics.

4.2 Main Results

We present quantitative comparisons of different methods in Table 2 and visual comparisons in Figs. 2, 3 (and Figs. 5, 6, 7 in the Appendix A.4). Overall, our method achieves the best quantitative (*on average*) and qualitative performance across all compared methods.

First, while Self2Self excels on PolyU and CC datasets, it shows poor denoising capacity (both PSNR/SSIM values and visual results) on SIDD and FMDD that contain severe image noise, as shown in Fig. 5. PD-denoising is generally effective but often introduces small artifacts that hinder visual effects, as seen in Fig. 5. ZS-N2N struggles with real-world noisy images and typically leaves noticeable noise after denoising due to its reliance on the independent noise assumption. Regarding diffusion priors-based methods, GDP and GR2 perform poorly on real-world denoising, introducing artifacts (see Figs 5a and 7) and over-smoothing (see Fig. 3), possibly because they adopt hard data-consistency methods, which significantly deviate from the true likelihood function. As DDRM assumes Gaussian white noise, the denoised images often retain some noise, which cannot be entirely removed, as shown in Figs 3 and 5b. ScoreDVI is the most competitive method against ours, but it sometimes blurs images and loses local textures, as indicated by Fig. 2. Unlike these methods, our approach effectively removes severe noise while preserving image details and textures.

Table 2: Quantitative comparisons (PSNR(dB)/SSIM) of different methods on diverse real-world image datasets. The best and second-best PSNR/SSIM results are marked in **bold** and <u>underlined</u>.

Methods	SIDD Validation [1]	FMDD [51]	PolyU [47]	CC [30]	Average
DIP [42]	32.11/0.740	32.90/0.854	37.17/0.912	35.61/0.912	34.45/0.855
Self2Self [36]	29.46/0.595	30.76/0.695	<u>38.33/0.962</u>	<u>37.45/0.948</u>	34.00/0.800
PD-denoising [52]	33.97/0.820	33.01/0.856	37.04/0.940	35.85/0.923	34.97/0.885
ZS-N2N [27]	25.58/0.433	31.61/0.767	36.05/0.916	33.58/0.854	31.71/0.743
ScoreDVI [7]	34.75/0.856	<u>33.10</u>/**0.865**	37.77/0.959	37.09/0.945	<u>35.68/0.906</u>
GDP [12]	27.65/0.615	27.68/0.698	32.30/0.905	31.45/0.916	29.77/0.784
DR2 [45]	32.02/0.728	30.52/0.813	34.37/0.925	32.30/0.876	32.30/0.836
DDRM [19]	33.14/0.796	32.54/0.837	33.14/0.767	36.04/0.923	33.72/0.831
Ours	<u>34.76</u>/**0.887**	**33.14**/<u>0.860</u>	**38.71/0.970**	**38.01/0.959**	**36.16/0.919**
APBSN [23]	**36.80**/<u>0.874</u>	31.99/0.836	37.03/0.951	34.88/0.925	35.18/0.897

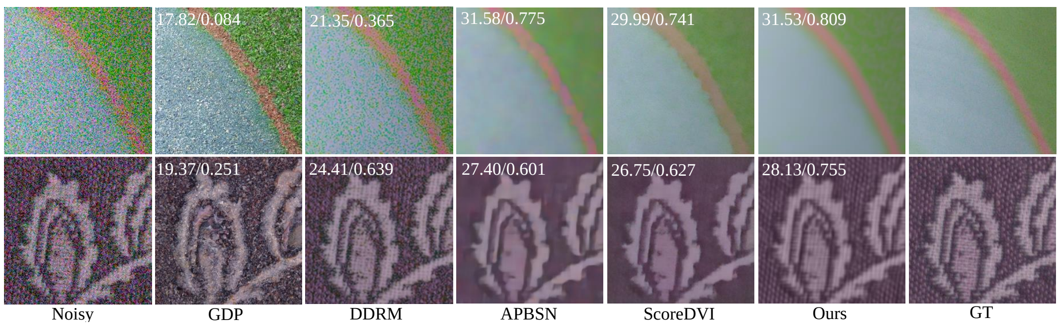

Figure 2: Visual comparison of different denoising methods in SIDD validation dataset.

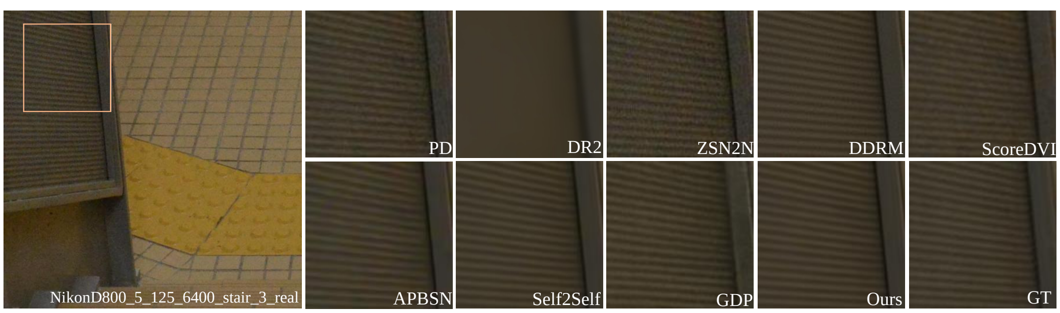

Figure 3: Visual comparison of different denoising methods in PolyU. PSNR/SSIM values: PD (36.77/0.916), APBSN (37.59/0.944), DR2 (34.53/0.864), Self2Self (39.44/0.961), ZSN2N (35.12/0.879), GDP (33.43/0.888), DDRM (33.61/0.773), ScoreDVI (37.76/0.939), Ours (39.01/0.965)

Although APBSN achieves the best PSNR values in the SIDD dataset, it frequently introduces noticeable color artifacts (see Figs. 2, 3) and oversmooths images (see Fig. 7). In addition, when applied to FMDD, PolyU, and CC datasets that contain fewer noisy images, its denoising performance significantly degrades and underperforms our method. This highlights the advantage of our data-efficient approach.

4.3 Ablation and Analyses

Adaptive likelihood estimation (ALE). We analyze $1/\mathrm{E}(\phi_0) = \hat{\beta}_0/\hat{\alpha}_0$, the estimated noise variance, and present quantitative and qualitative results in Fig. 4. Fig. 4a demonstrates that $\hat{\beta}_0/\hat{\alpha}_0$ effectively reflects the noise variance of y_0. That is, $\hat{\beta}_0/\hat{\alpha}_0$ exhibits larger values in noisier areas of y_0 and smaller values (black) in less noisy areas. Fig. 4b implies that the average of $\hat{\beta}_0/\hat{\alpha}_0$ are inversely correlated with PSNR values of denoised images, which is reasonable since noisier images are more challenging to denoise and hence have lower PSNR. Conversely, the prior noise variance $\beta/\alpha = 3e^{-3}$,

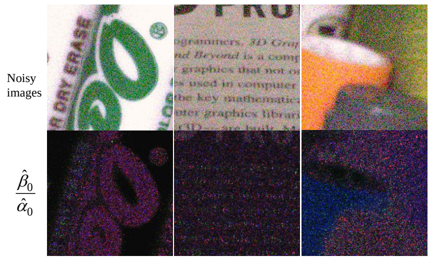

(a) Visual results of $\hat{\beta}_0/\hat{\alpha}_0$

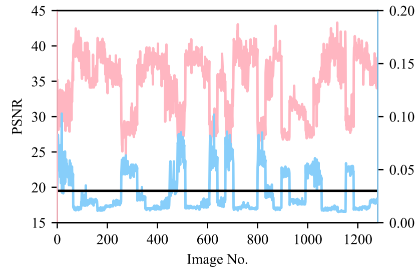

(b) PSNR vs average $\hat{\beta}_0/\hat{\alpha}_0$.

Figure 4: The estimated noise variance $1/\mathrm{E}(\phi_0) = \hat{\beta}_0/\hat{\alpha}_0$ on SIDD dataset

Table 3: Ablation on adaptive likelihood estimation and local Gaussian convolution

with ALE	with Gaussian Conv	SIDD	FMDD	PolyU	CC
✗	✗	32.12/0.741	27.07/0.530	35.40/0.895	33.10/0.830
✓	✗	34.63/0.870	33.11/**0.865**	38.70/0.969	37.82/0.956
✓	✓	**34.76/0.887**	**33.14**/0.860	**38.71/0.970**	**38.01/0.959**

indicated by the black plot in Fig. 4b are constant for all noisy images. These analyses suggest that the ALE captures the signal-dependent features of real-world noise effectively.

In addition, we skip the variational inference process and directly use the prior precision $p(\phi_{t-1})$ to derive x^*_{t-1}, resulting in $x^*_{t-1} = \pi_{t-1}y_{t-1} + (1-\pi_{t-1})\mu_\theta(x_t,t), \pi_{t-1} = \sigma_t^2\alpha/(\sigma_t^2\alpha+\beta)$. The corresponding denoising result (i.e., without ALE) is reported in the second row of Table 3 and is largely behind the denoising result of using ALE, further verifying the effectiveness of ALE.

Rectification in Eq. (17). By introducing the local Gaussian convolution operation, we explicitly refine the estimated noise variance $1/\mathrm{E}(\phi_{t-1})$. As shown in the fourth row of Table 3, using $\overline{1/\mathrm{E}(\phi_{t-1})}$ consistently improves the quantitative performance.

Table 4: Ablation of temperature γ on CC dataset

γ value	1	$1/2$	$1/4$
PSNR/SSIM	37.74/0.955	37.73/0.955	37.90/0.957
γ value	$1/5$	$1/10$	$1/20$
PSNR/SSIM	**38.01/0.959**	37.80/0.953	35.55/0.913

Table 5: Ablation of β and s on CC dataset

β value	5e-3	1e-2	1.5e-2
PSNR/SSIM	38.03/0.957	38.01/0.959	37.47/0.953
s value	0.8	1.0	1.2
PSNR/SSIM	37.876/0.957	38.01/0.959	38.10/0.959

Table 6: Denoising performance of using diffusion priors pre-trained with other image resolutions

Res.: Train → Test	SIDD	Res.: Train → Test	CC	PolyU	FMDD
128 → 256	**34.80**/0.836	256 → 512	**38.01/0.959**	**38.71/0.970**	**33.14/0.860**
256 → 256	34.76/**0.887**	512 → 512	37.01/0.950	38.33/0.966	33.02/0.859

Temperature γ. When $\gamma \leq 1$, the effect of diffusion priors $p(x_{t-1}|x_t)$ is reduced within the variational inference during the reverse diffusion process. As shown in Table 4, decreasing γ gradually improves the quantitative denoising performance, peaking at $\gamma = 1/5$. Further reducing γ degrades PSNR/SSIM as insufficient diffusion priors are involved in variational Bayes.

β **in prior precision and kernel scale** s. Regarding β, it roughly represents the noise level of noisy image y (given $\alpha = 1$) and we choose β according to the empirical variance of the textureless area of y for one test set. kernel scale s is set by considering the spatial correlation of noise present in real-world images. We ablate these two parameters in Table 5, which indicates that they are relatively robust to moderate changes.

Local diffusion priors. We consider diffusion models pre-trained with other image resolutions as diffusion priors, including the 128×128 version and 512×512 version [4]. The corresponding denoising performance is reported in Table 6, and implementation details are provided in the Appendix A.3.1. Regarding SIDD, we observe that matching the resolution of diffusion priors and test images (both 256×256) achieves the best performance. Such a result is reversed for the remaining datasets,

[4]https://openaipublic.blob.core.windows.net/diffusion/jul-2021/512x512_diffusion.pt

Table 7: The quantitative performance on removing other non-Gaussian synthetic noises

CBSD68 [28]	Poisson ($\lambda = 30$)	Bernoulli ($p = 0.2$)	KodaK [13]	Poisson ($\lambda = 30$)	Bernoulli ($p = 0.2$)
ZS-N2N	27.55/0.781	20.20/**0.828**	ZS-N2N	28.09/0.750	19.98/**0.820**
Ours	**29.24/0.833**	**26.11**/0.784	Ours	**30.56/0.839**	**27.17**/0.799

where the 256×256 diffusion prior for HR images is more effective than its 512×512 counterpart. This is likely because training HR diffusion models (e.g., ≥ 512) is more challenging, resulting in inferior generation performance (e.g., FID) compared to LR diffusion models [9]. Consequently, the local prior inherent in medium-resolution diffusion models is superior for restoring HR images.

4.4 Application to other non-Gaussian noises

Although our method is designed to handle real-world noise, it can also address other non-Gaussian noises, including Poisson noise and multiplicative Bernoulli noise. As these synthetic noises are spatially independent, we do not utilize Eq. (17) in our method. We report the denoising performance in Table 7, with ZS-N2N [16] selected for comparison. Experimental details and visual results are given in the Appendix A.3.2 and A.5. Our method achieves better quantitative metrics than ZS-N2N on Poisson denoising and also preserves more local details and textures (see Fig. 8). While ZS-N2N shows better SSIM than ours on Bernoulli denoising, it causes intensity shifts (see Fig. 9) and thus has poorer PSNR.

4.5 Application to image demosaicing

In addition to denoising, our method is readily available for image restoration with pixel-wise degradation, e.g., image demosaicing. To adapt our method to this task, we define the forward process $y_0 = M \odot x_0$, where M is the degradation operator, and denotes element-wise multiplication. For demosaicing, M is the binary mask with 0 values indicating missing pixels of y_0. We can incorporate M into $p(y_{t-1}|x_{t-1}, \phi_{t-1})$ in Eq. (15), which results in $\hat{\pi}_{t-1} = \frac{M\sigma_t^2}{M\sigma_t^2 + 1/\mathrm{E}(\phi_{t-1})}$. In Table 8, we compare our method against DDRM on image demosaicing (CFA pattern: RGGB), and our method shows better results.

Table 8: Results of image demosaicing

Dataset	Set14	CBSD68
DDRM	24.68/0.714	24.52/0.705
Ours	**26.02/0.756**	**25.43/0.732**

Table 9: Results of different sampling steps

Step	1000	500	250
SIDD Val	**34.76/0.887**	33.54/0.838	23.89/0.825
CC	**38.01/0.959**	37.18/0.947	22.72/0.716

Limitation. Our method builds on the DDPM sampling with a total of 1000 diffusion steps. Denoising a single noisy image with a resolution of 256×256 on an Nvidia 2080Ti GPU takes approximately 230 seconds, which is inefficient. In comparison, ZS-N2N takes about 16 seconds, despite its inferior denoising performance. Naively reducing diffusion steps in our method leads to apparent performance decreases, as indicated in Table 9. Our next move is to incorporate advanced accelerated sampling strategies into our method to reduce inference time while maintaining performance.

5 Conclusion

In this paper, we built upon diffusion priors and variational Bayes and proposed adaptive likelihood estimation and MAP inference during the reverse diffusion process, to handle real-world image noise that is structured and signal-dependent. The employed $i.ni.d.$ likelihood function, combined with the precision prior and variational Bayes, allowed for the dynamical update of $i.ni.d.$ noise precision posterior in each step of the generation process. This strategy adaptively refined the likelihood function and enabled the better MAP inference. Our method achieved excellent denoising performance on diverse real-world image denoising datasets and was also effective for removing other non-Gaussian synthetic noises.

Acknowledgment

This work was supported in part by the National Natural Science Foundation of China (NNSFC), under Grant Nos. 61672253, 62071197, and 62471192.

References

[1] Abdelrahman Abdelhamed, Stephen Lin, and Michael S Brown. A high-quality denoising dataset for smartphone cameras. In *CVPR*, pages 1692–1700, 2018.

[2] Laurence Aitchison. A statistical theory of cold posteriors in deep neural networks. In *ICLR*, 2021.

[3] Joshua Batson and Loic Royer. Noise2self: Blind denoising by self-supervision. In *ICML*, pages 524–533. PMLR, 2019.

[4] Christopher M Bishop and Nasser M Nasrabadi. *Pattern recognition and machine learning*, volume 4. Springer, 2006.

[5] Gabriel Cardoso, Sylvain Le Corff, Eric Moulines, et al. Monte carlo guided denoising diffusion models for bayesian linear inverse problems. In *ICLR*, 2024.

[6] Hao Chen, Chenyuan Qu, Yu Zhang, Chen Chen, and Jianbo Jiao. Multi-view self-supervised disentanglement for general image denoising. In *ICCV*, pages 12281–12291, 2023.

[7] Jun Cheng, Tao Liu, and Shan Tan. Score priors guided deep variational inference for unsupervised real-world single image denoising. In *ICCV*, pages 12937–12948, 2023.

[8] Hyungjin Chung, Jeongsol Kim, Michael Thompson Mccann, Marc Louis Klasky, and Jong Chul Ye. Diffusion posterior sampling for general noisy inverse problems. In *ICLR*, 2023.

[9] Prafulla Dhariwal and Alexander Nichol. Diffusion models beat gans on image synthesis. *NeurIPS*, 34:8780–8794, 2021.

[10] Zehao Dou and Yang Song. Diffusion posterior sampling for linear inverse problem solving: A filtering perspective. In *ICLR*, 2024.

[11] Wenchao Du, Hu Chen, and Hongyu Yang. Learning invariant representation for unsupervised image restoration. In *CVPR*, pages 14483–14492, 2020.

[12] Ben Fei, Zhaoyang Lyu, Liang Pan, Junzhe Zhang, Weidong Yang, Tianyue Luo, Bo Zhang, and Bo Dai. Generative diffusion prior for unified image restoration and enhancement. In *CVPR*, pages 9935–9946, 2023.

[13] Rich Franzen. Kodak lossless true color image suite. http://r0k.us/graphics/kodak/, 1999.

[14] Jonathan Ho, Ajay Jain, and Pieter Abbeel. Denoising diffusion probabilistic models. *NeurIPS*, 33:6840–6851, 2020.

[15] Emiel Hoogeboom, Jonathan Heek, and Tim Salimans. simple diffusion: End-to-end diffusion for high resolution images. In *ICLM*, pages 13213–13232. PMLR, 2023.

[16] Tao Huang, Songjiang Li, Xu Jia, Huchuan Lu, and Jianzhuang Liu. Neighbor2neighbor: Self-supervised denoising from single noisy images. In *CVPR*, pages 14781–14790, 2021.

[17] Geonwoon Jang, Wooseok Lee, Sanghyun Son, and Kyoung Mu Lee. C2n: Practical generative noise modeling for real-world denoising. In *ICCV*, pages 2350–2359, 2021.

[18] Jari Kaipio and Erkki Somersalo. *Statistical and computational inverse problems*, volume 160. Springer Science & Business Media, 2006.

[19] Bahjat Kawar, Michael Elad, Stefano Ermon, and Jiaming Song. Denoising diffusion restoration models. *NeurIPS*, 35:23593–23606, 2022.

[20] Kwanyoung Kim and Jong Chul Ye. Noise2score: tweedie's approach to self-supervised image denoising without clean images. *NeurIPS*, 34:864–874, 2021.

[21] Shayan Kousha, Ali Maleky, Michael S Brown, and Marcus A Brubaker. Modeling srgb camera noise with normalizing flows. In *CVPR*, pages 17463–17471, 2022.

[22] Samuli Laine, Tero Karras, Jaakko Lehtinen, and Timo Aila. High-quality self-supervised deep image denoising. *NeurIPS*, 32, 2019.

[23] Wooseok Lee, Sanghyun Son, and Kyoung Mu Lee. Ap-bsn: Self-supervised denoising for real-world images via asymmetric pd and blind-spot network. In *CVPR*, pages 17725–17734, 2022.

[24] Xin Li, Yulin Ren, Xin Jin, Cuiling Lan, Xingrui Wang, Wenjun Zeng, Xinchao Wang, and Zhibo Chen. Diffusion models for image restoration and enhancement–a comprehensive survey. *arXiv preprint arXiv:2308.09388*, 2023.

[25] Yawei Li, Yuchen Fan, Xiaoyu Xiang, Denis Demandolx, Rakesh Ranjan, Radu Timofte, and Luc Van Gool. Efficient and explicit modelling of image hierarchies for image restoration. In *CVPR*, pages 18278–18289, 2023.

[26] A.C. Likas and N.P. Galatsanos. A variational approach for bayesian blind image deconvolution. *IEEE Transactions on Signal Processing*, 52(8):2222–2233, 2004.

[27] Youssef Mansour and Reinhard Heckel. Zero-shot noise2noise: Efficient image denoising without any data. In *CVPR*, pages 14018–14027, 2023.

[28] David Martin, Charless Fowlkes, Doron Tal, and Jitendra Malik. A database of human segmented natural images and its application to evaluating segmentation algorithms and measuring ecological statistics. In *ICCV*, volume 2, pages 416–423. IEEE, 2001.

[29] Nick Moran, Dan Schmidt, Yu Zhong, and Patrick Coady. Noisier2noise: Learning to denoise from unpaired noisy data. In *CVPR*, pages 12064–12072, 2020.

[30] Seonghyeon Nam, Youngbae Hwang, Yasuyuki Matsushita, and Seon Joo Kim. A holistic approach to cross-channel image noise modeling and its application to image denoising. In *CVPR*, pages 1683–1691, 2016.

[31] Reyhaneh Neshatavar, Mohsen Yavartanoo, Sanghyun Son, and Kyoung Mu Lee. Cvf-sid: Cyclic multi-variate function for self-supervised image denoising by disentangling noise from image. In *CVPR*, pages 17583–17591, 2022.

[32] Xingang Pan, Xiaohang Zhan, Bo Dai, Dahua Lin, Chen Change Loy, and Ping Luo. Exploiting deep generative prior for versatile image restoration and manipulation. *TPAMI*, 44(11):7474–7489, 2021.

[33] Yizhong Pan, Xiao Liu, Xiangyu Liao, Yuanzhouhan Cao, and Chao Ren. Random sub-samples generation for self-supervised real image denoising. In *ICCV*, pages 12150–12159, 2023.

[34] Tongyao Pang, Huan Zheng, Yuhui Quan, and Hui Ji. Recorrupted-to-recorrupted: unsupervised deep learning for image denoising. In *CVPR*, pages 2043–2052, 2021.

[35] Mangal Prakash, Mauricio Delbracio, Peyman Milanfar, and Florian Jug. Interpretable unsupervised diversity denoising and artefact removal. In *ICLR*, 2022.

[36] Yuhui Quan, Mingqin Chen, Tongyao Pang, and Hui Ji. Self2self with dropout: Learning self-supervised denoising from single image. In *CVPR*, pages 1890–1898, 2020.

[37] Robin Rombach, Andreas Blattmann, Dominik Lorenz, Patrick Esser, and Björn Ommer. High-resolution image synthesis with latent diffusion models. In *CVPR*, pages 10684–10695, 2022.

[38] Shakarim Soltanayev and Se Young Chun. Training deep learning based denoisers without ground truth data. *NeurIPS*, 31, 2018.

[39] Yang Song, Liyue Shen, Lei Xing, and Stefano Ermon. Solving inverse problems in medical imaging with score-based generative models. In *ICLR*, 2022.

[40] Yang Song, Jascha Sohl-Dickstein, Diederik P Kingma, Abhishek Kumar, Stefano Ermon, and Ben Poole. Score-based generative modeling through stochastic differential equations. In *ICLR*, 2020.

[41] Jiayan Teng, Wendi Zheng, Ming Ding, Wenyi Hong, Jianqiao Wangni, Zhuoyi Yang, and Jie Tang. Relay diffusion: Unifying diffusion process across resolutions for image synthesis. In *ICLR*, 2024.

[42] Dmitry Ulyanov, Andrea Vedaldi, and Victor Lempitsky. Deep image prior. In *CVPR*, pages 9446–9454, 2018.

[43] Yinhuai Wang, Jiwen Yu, and Jian Zhang. Zero-shot image restoration using denoising diffusion null-space model. In *ICLR*, 2023.

[44] Zejin Wang, Jiazheng Liu, Guoqing Li, and Hua Han. Blind2unblind: Self-supervised image denoising with visible blind spots. In *CVPR*, pages 2027–2036, 2022.

[45] Zhixin Wang, Ziying Zhang, Xiaoyun Zhang, Huangjie Zheng, Mingyuan Zhou, Ya Zhang, and Yanfeng Wang. Dr2: Diffusion-based robust degradation remover for blind face restoration. In *CVPR*, pages 1704–1713, 2023.

[46] Zichun Wang, Ying Fu, Ji Liu, and Yulun Zhang. Lg-bpn: Local and global blind-patch network for self-supervised real-world denoising. In *CVPR*, pages 18156–18165, 2023.

[47] Jun Xu, Hui Li, Zhetong Liang, David Zhang, and Lei Zhang. Real-world noisy image denoising: A new benchmark. *arXiv preprint arXiv:1804.02603*, 2018.

[48] Zongsheng Yue, Hongwei Yong, Qian Zhao, Deyu Meng, and Lei Zhang. Variational denoising network: Toward blind noise modeling and removal. *NeurIPS*, 32, 2019.

[49] Syed Waqas Zamir, Aditya Arora, Salman Khan, Munawar Hayat, Fahad Shahbaz Khan, and Ming-Hsuan Yang. Restormer: Efficient transformer for high-resolution image restoration. In *CVPR*, pages 5728–5739, 2022.

[50] Kai Zhang, Wangmeng Zuo, Yunjin Chen, Deyu Meng, and Lei Zhang. Beyond a gaussian denoiser: Residual learning of deep cnn for image denoising. *TIP*, 26(7):3142–3155, 2017.

[51] Yide Zhang, Yinhao Zhu, Evan Nichols, Qingfei Wang, Siyuan Zhang, Cody Smith, and Scott Howard. A poisson-gaussian denoising dataset with real fluorescence microscopy images. In *CVPR*, pages 11710–11718, 2019.

[52] Yuqian Zhou, Jianbo Jiao, Haibin Huang, Yang Wang, Jue Wang, Honghui Shi, and Thomas Huang. When awgn-based denoiser meets real noises. In *AAAI*, pages 13074–13081, 2020.

A Appendix

A.1 Derivation of Eq. (6)

As analyzed in Section 3.2, in principle we can model the likelihood function of real-world noisy images as $p(y_0|x_0) = \mathcal{N}(x_0, \Sigma(x_0))$, where Σ is a non-diagonal covariance matrix and its variance is related to its mean x_0 (or signal). In order to incorporate y_0 into the inverse diffusion process and shorten its gap to x_{t-1}, we can construct y_{t-1} based Eq. (2) to obtain $y_{t-1} = \sqrt{\bar{\alpha}_{t-1}}y_0 + \sqrt{1-\bar{\alpha}_{t-1}}\epsilon_2$. For y_0, it can be sampled from the multi-variate Gaussian $p(y_0|x_0) = \mathcal{N}(x_0, \Sigma(x_0))$, i.e., $y_0 = x_0 + A\epsilon$, where $AA^T = \Sigma(x_0)$, and A is obtained by Cholesky decomposition. Finally, we obtain

$$\begin{aligned} y_{t-1} &= \sqrt{\bar{\alpha}_{t-1}}y_0 + \sqrt{1-\bar{\alpha}_{t-1}}\epsilon = \sqrt{\bar{\alpha}_{t-1}}(x_0 + A\epsilon_2) + \sqrt{1-\bar{\alpha}_{t-1}}\epsilon \\ &= \sqrt{\bar{\alpha}_{t-1}}x_0 + \sqrt{1-\bar{\alpha}_{t-1}}\epsilon + \sqrt{\bar{\alpha}_{t-1}}A\epsilon_2 = x_{t-1} + \sqrt{\bar{\alpha}_{t-1}}A\epsilon_2 \end{aligned} \tag{18}$$

A.2 Derivations of Eqs. (11) and (13)

Regarding Eq. (10), we have

$$\begin{aligned} &\mathrm{E}_{\phi_{t-1}} \log p(y_{t-1}|x_{t-1},\phi_{t-1})^{\frac{1}{\gamma}} p(x_{t-1}|x_t)p(\phi_{t-1}) \\ &=\mathrm{E}_{\phi_{t-1}} \sum_{i=1}^{N} \left(-\frac{(y_{t-1}^i - x_{t-1}^i)^2}{2\gamma}\phi_{t-1}^i - \frac{(x_{t-1}^i - \mu_t^i)^2}{2\sigma_t^2} \right) + \mathrm{const} \\ &= \sum_{i=1}^{N} \left(-\frac{(y_{t-1}^i - x_{t-1}^i)^2}{2\gamma}\mathrm{E}(\phi_{t-1}^i) - \frac{(x_{t-1}^i - \mu_t^i)^2}{2\sigma_t^2} \right) + \mathrm{const} \\ &= \sum_{i=1}^{N} -\frac{(y_{t-1}^i - x_{t-1}^i)^2 \mathrm{E}(\phi_{t-1}^i)\sigma_t^2 + (x_{t-1}^i - \mu_t^i)^2\gamma}{2\gamma\sigma_t^2} + \mathrm{const} \\ &= \sum_{i=1}^{N} -\frac{(\mathrm{E}(\phi_{t-1}^i)\sigma_t^2 + \gamma)(x_{t-1}^i)^2 - 2(\mathrm{E}(\phi_{t-1}^i)\sigma_t^2 y_{t-1}^i + \mu_t^i\gamma)x_{t-1}^i}{2\gamma\sigma_t^2} + \mathrm{const} \end{aligned} \tag{19}$$

where $\mu_t = \mu_\theta(x_t, t)$. We observe that Eq. (19) has the summation and quadratic form of x_{t-1}^i, and hence $g(x_{t-1})$ is identified as a diagonal Gaussian distribution. By completing the square, we can obtain

$$g(x_{t-1}) = \mathcal{N}\left(\frac{\sigma_t^2 \mathrm{E}(\phi_{t-1}) \odot y_{t-1} + \mu_t\gamma}{\mathrm{E}(\phi_{t-1})\sigma_t^2 + \gamma}, \mathrm{diag}\left(\frac{\gamma\sigma_t^2}{\mathrm{E}(\phi_{t-1})\sigma_t^2 + \gamma}\right)\right) \tag{20}$$

Similarly, given $g(x_{t-1})$, the optimal $g^*(\phi_{t-1})$ is provided by

$$\log g^*(\phi_{t-1}) = \mathrm{E}_{x_{t-1}} \log p(y_{t-1}|x_{t-1},\phi_{t-1})^{\frac{1}{\gamma}} p(x_{t-1}|x_t)p(\phi_{t-1}) \tag{21}$$

which corresponds to

$$\begin{aligned} &\mathrm{E}_{x_{t-1}} \log p(y_{t-1}|x_{t-1},\phi_{t-1})^{\frac{1}{\gamma}} p(x_{t-1}|x_t)p(\phi_{t-1}) \\ =&\mathrm{E}_{x_{t-1}} \sum_{i=1}^{N} \left(\frac{1}{2\gamma}\log\phi_{t-1}^i - \frac{(y_{t-1}^i - x_{t-1}^i)^2}{2\gamma}\phi_{t-1}^i + (\alpha_{t-1}-1)\log\phi_{t-1}^i - \beta_{t-1}\phi_{t-1}^i \right) + \mathrm{const} \\ =& \sum_{i=1}^{N} \left(\frac{1}{2\gamma}\log\phi_{t-1}^i - \frac{(y_{t-1}^i - \mathrm{E}(x_{t-1}^i))^2 + \sigma_t^2}{2\gamma}\phi_{t-1}^i + (\alpha_{t-1}-1)\log\phi_{t-1}^i - \beta_{t-1}\phi_{t-1}^i \right) + \mathrm{const} \end{aligned} \tag{22}$$

From Eq. (22), we identify each $g(\phi_{t-1}^i)$ is a independent gamma distribution and hence $g(\phi_{t-1})$ is

$$g^*(\phi_{t-1}) = \prod_{i=1}^{N} \mathrm{Gamma}\left(\phi_{t-1}^i; \alpha_{t-1} + \frac{1}{2\gamma}, \beta_{t-1} + \frac{(y_{t-1}^i - \hat{\mu}_{t-1}^i)^2 + (\hat{\sigma}_{t-1}^2)^i}{2\gamma}\right) \tag{23}$$

A.3 Additional implementation details

A.3.1 Applying class-conditional diffusion models as diffusion priors

We note that [9] only provides the 256×256 unconditional diffusion model $\epsilon_\theta(x_t, t)$ trained on ImageNet, and the remaining diffusion models are class-conditional, i.e., $\epsilon_\theta(x_t, c, t)$ with the class label c. There are two ways to utilize these class-conditional diffusion priors for image denoising. Regarding each noisy image, we first sample a class label c from $randint(0, 1000)$ and input it to the $\epsilon_\theta(x_t, c, t)$ combined with x_t and t. One way is then ignoring the guidance from the pre-trained classifier during the generation process and directly computing $\mu_\theta(x_t, t)$ based on $\epsilon_\theta(x_t, c, t)$ and Eq. (4). The other way is further updating $\mu_\theta(x_t, t)$ to $\mu_\theta(x_t, t) + g_s \sigma_t^2 \nabla_{x_t} \log p_\psi(c|x_t)$, where $p_\psi(c|x_t)$ is the classifier and g_s is the guidance scale. Basically, we found these two ways resulted in similar denoising performance, and Table 6 used the first way.

A.3.2 Experiments on denoising non-Gaussian synthetic noises

Synthesis of noisy images. Regarding Bernoulli noise, we obtain the noisy image by $y_0 = x_0 \odot M, M =$ torch.bernoulli(torch.ones_like(x_0) $* p$), $p = 0.2$; Regarding Poisson noise, we obtain the noisy image by $y_0 =$ torch.poisson($\lambda * x_0$)$/\lambda, \lambda = 30$.

Hyperparameters. For our method, we set $\beta = 1e^{-2}$ and $\beta = 8e^{-3}$ for Bernoulli noise and Poisson noise removal, respectively. The remaining hyperparameters are identical to those of our main experiments.

A.4 Visual comparisons of denoising results on real-world datasets

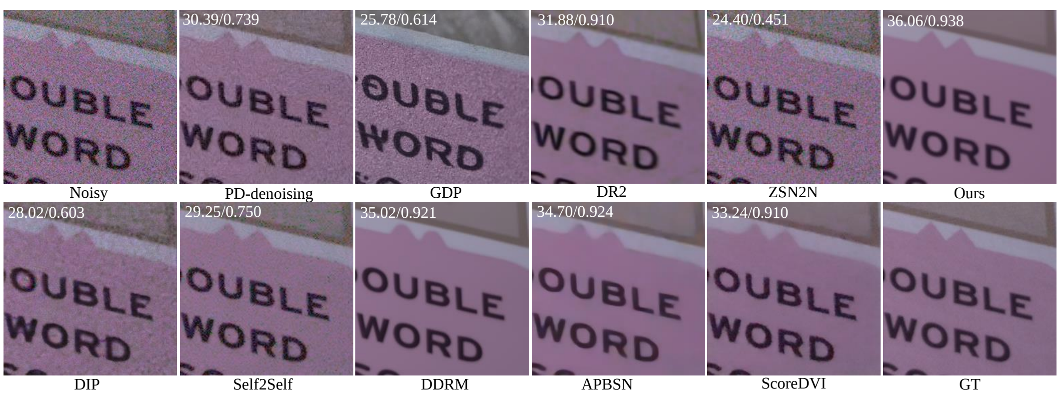

(a) Denoising result of 34_14.png

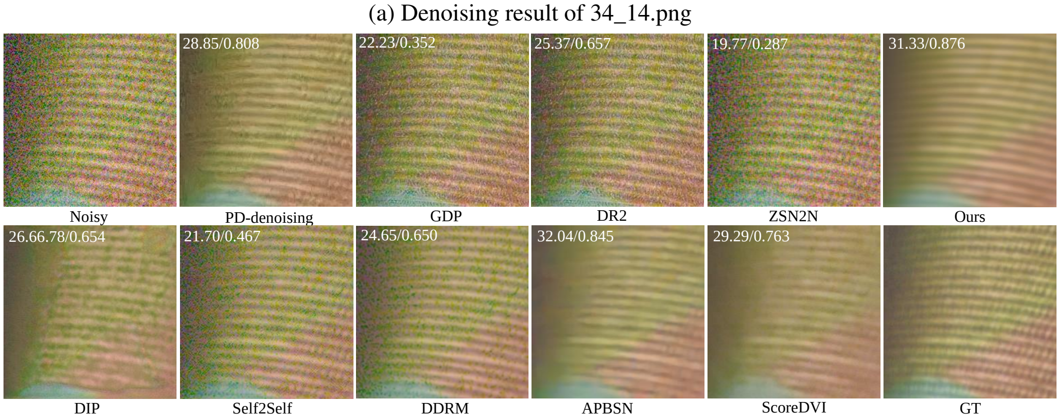

(b) Denoising result of 10_6.png

Figure 5: Visual comparison of different denoising methods in SIDD validation dataset.

A.5 Visual comparisons of denoising results on synthetic noises

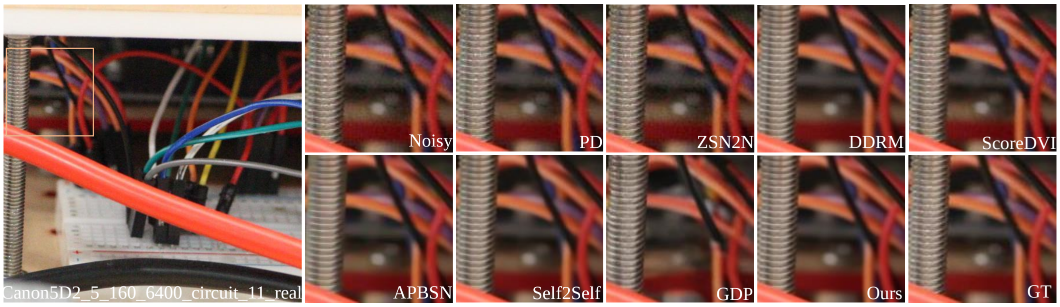

Figure 6: Visual comparison of different denoising methods in PolyU.

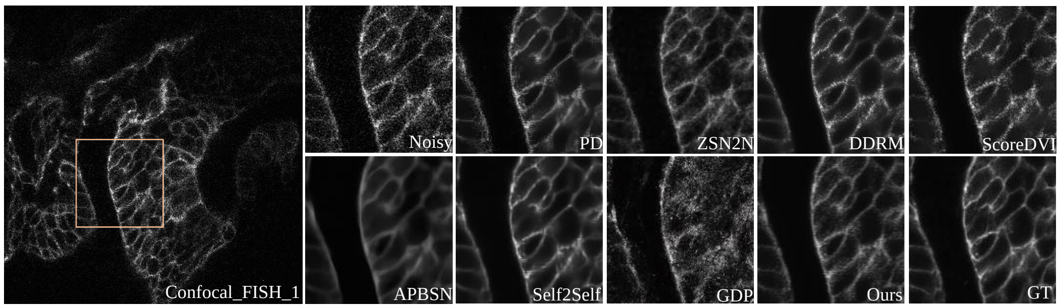

Figure 7: Visual comparison of different denoising methods in FMDD.

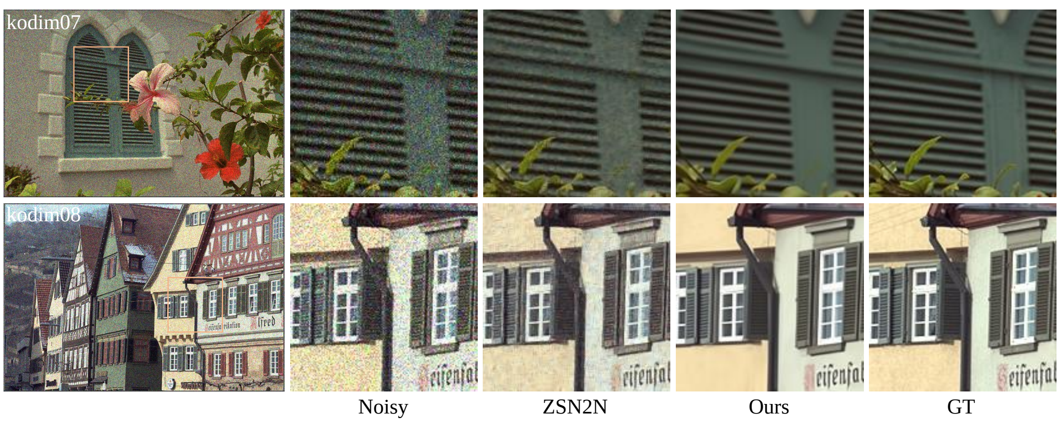

Figure 8: Visual comparison of denoising results on Poisson denoising ($\lambda = 30$)

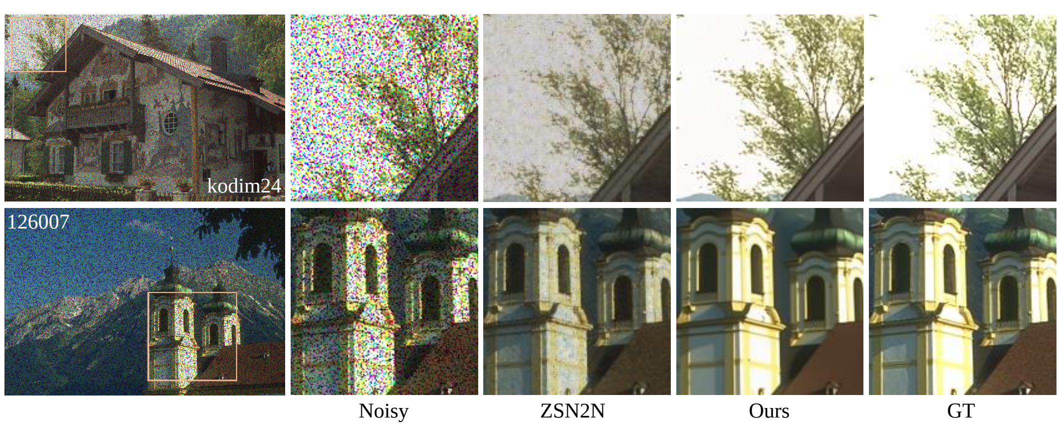

Figure 9: Visual comparison of denoising results on Bernoulli denoising ($p = 0.2$)

NeurIPS Paper Checklist

1. **Claims**

   Question: Do the main claims made in the abstract and introduction accurately reflect the paper's contributions and scope?

   Answer: [Yes]

   Justification: see the abstract and introduction in the main text

   Guidelines:

   - The answer NA means that the abstract and introduction do not include the claims made in the paper.
   - The abstract and/or introduction should clearly state the claims made, including the contributions made in the paper and important assumptions and limitations. A No or NA answer to this question will not be perceived well by the reviewers.
   - The claims made should match theoretical and experimental results, and reflect how much the results can be expected to generalize to other settings.
   - It is fine to include aspirational goals as motivation as long as it is clear that these goals are not attained by the paper.

2. **Limitations**

   Question: Does the paper discuss the limitations of the work performed by the authors?

   Answer: [Yes]

   Justification: We discussed the limitation of our method in the main paper

   Guidelines:

   - The answer NA means that the paper has no limitation while the answer No means that the paper has limitations, but those are not discussed in the paper.
   - The authors are encouraged to create a separate "Limitations" section in their paper.
   - The paper should point out any strong assumptions and how robust the results are to violations of these assumptions (e.g., independence assumptions, noiseless settings, model well-specification, asymptotic approximations only holding locally). The authors should reflect on how these assumptions might be violated in practice and what the implications would be.
   - The authors should reflect on the scope of the claims made, e.g., if the approach was only tested on a few datasets or with a few runs. In general, empirical results often depend on implicit assumptions, which should be articulated.
   - The authors should reflect on the factors that influence the performance of the approach. For example, a facial recognition algorithm may perform poorly when image resolution is low or images are taken in low lighting. Or a speech-to-text system might not be used reliably to provide closed captions for online lectures because it fails to handle technical jargon.
   - The authors should discuss the computational efficiency of the proposed algorithms and how they scale with dataset size.
   - If applicable, the authors should discuss possible limitations of their approach to address problems of privacy and fairness.
   - While the authors might fear that complete honesty about limitations might be used by reviewers as grounds for rejection, a worse outcome might be that reviewers discover limitations that aren't acknowledged in the paper. The authors should use their best judgment and recognize that individual actions in favor of transparency play an important role in developing norms that preserve the integrity of the community. Reviewers will be specifically instructed to not penalize honesty concerning limitations.

3. **Theory Assumptions and Proofs**

   Question: For each theoretical result, does the paper provide the full set of assumptions and a complete (and correct) proof?

   Answer: [Yes]

Justification: We provided the derivations of related equations in **??**

Guidelines:

- The answer NA means that the paper does not include theoretical results.
- All the theorems, formulas, and proofs in the paper should be numbered and cross-referenced.
- All assumptions should be clearly stated or referenced in the statement of any theorems.
- The proofs can either appear in the main paper or the supplemental material, but if they appear in the supplemental material, the authors are encouraged to provide a short proof sketch to provide intuition.
- Inversely, any informal proof provided in the core of the paper should be complemented by formal proofs provided in appendix or supplemental material.
- Theorems and Lemmas that the proof relies upon should be properly referenced.

4. **Experimental Result Reproducibility**

   Question: Does the paper fully disclose all the information needed to reproduce the main experimental results of the paper to the extent that it affects the main claims and/or conclusions of the paper (regardless of whether the code and data are provided or not)?

   Answer: [Yes]

   Justification: We presented detailed experimental settings in Section 4.1

   Guidelines:

   - The answer NA means that the paper does not include experiments.
   - If the paper includes experiments, a No answer to this question will not be perceived well by the reviewers: Making the paper reproducible is important, regardless of whether the code and data are provided or not.
   - If the contribution is a dataset and/or model, the authors should describe the steps taken to make their results reproducible or verifiable.
   - Depending on the contribution, reproducibility can be accomplished in various ways. For example, if the contribution is a novel architecture, describing the architecture fully might suffice, or if the contribution is a specific model and empirical evaluation, it may be necessary to either make it possible for others to replicate the model with the same dataset, or provide access to the model. In general. releasing code and data is often one good way to accomplish this, but reproducibility can also be provided via detailed instructions for how to replicate the results, access to a hosted model (e.g., in the case of a large language model), releasing of a model checkpoint, or other means that are appropriate to the research performed.
   - While NeurIPS does not require releasing code, the conference does require all submissions to provide some reasonable avenue for reproducibility, which may depend on the nature of the contribution. For example
     (a) If the contribution is primarily a new algorithm, the paper should make it clear how to reproduce that algorithm.
     (b) If the contribution is primarily a new model architecture, the paper should describe the architecture clearly and fully.
     (c) If the contribution is a new model (e.g., a large language model), then there should either be a way to access this model for reproducing the results or a way to reproduce the model (e.g., with an open-source dataset or instructions for how to construct the dataset).
     (d) We recognize that reproducibility may be tricky in some cases, in which case authors are welcome to describe the particular way they provide for reproducibility. In the case of closed-source models, it may be that access to the model is limited in some way (e.g., to registered users), but it should be possible for other researchers to have some path to reproducing or verifying the results.

5. **Open access to data and code**

   Question: Does the paper provide open access to the data and code, with sufficient instructions to faithfully reproduce the main experimental results, as described in supplemental material?

Answer: [Yes]

Justification: The source code is provided at https://github.com/HUST-Tan/DiffusionVI

Guidelines:

- The answer NA means that paper does not include experiments requiring code.
- Please see the NeurIPS code and data submission guidelines (https://nips.cc/public/guides/CodeSubmissionPolicy) for more details.
- While we encourage the release of code and data, we understand that this might not be possible, so "No" is an acceptable answer. Papers cannot be rejected simply for not including code, unless this is central to the contribution (e.g., for a new open-source benchmark).
- The instructions should contain the exact command and environment needed to run to reproduce the results. See the NeurIPS code and data submission guidelines (https://nips.cc/public/guides/CodeSubmissionPolicy) for more details.
- The authors should provide instructions on data access and preparation, including how to access the raw data, preprocessed data, intermediate data, and generated data, etc.
- The authors should provide scripts to reproduce all experimental results for the new proposed method and baselines. If only a subset of experiments are reproducible, they should state which ones are omitted from the script and why.
- At submission time, to preserve anonymity, the authors should release anonymized versions (if applicable).
- Providing as much information as possible in supplemental material (appended to the paper) is recommended, but including URLs to data and code is permitted.

6. **Experimental Setting/Details**

   Question: Does the paper specify all the training and test details (e.g., data splits, hyperparameters, how they were chosen, type of optimizer, etc.) necessary to understand the results?

   Answer: [Yes]

   Justification: We presented detailed experimental settings in Section 4.1

   Guidelines:

   - The answer NA means that the paper does not include experiments.
   - The experimental setting should be presented in the core of the paper to a level of detail that is necessary to appreciate the results and make sense of them.
   - The full details can be provided either with the code, in appendix, or as supplemental material.

7. **Experiment Statistical Significance**

   Question: Does the paper report error bars suitably and correctly defined or other appropriate information about the statistical significance of the experiments?

   Answer: [No]

   Justification: We did not report the statistical significance as our method mainly used real-world datasets rather than synthetic datasets.

   Guidelines:

   - The answer NA means that the paper does not include experiments.
   - The authors should answer "Yes" if the results are accompanied by error bars, confidence intervals, or statistical significance tests, at least for the experiments that support the main claims of the paper.
   - The factors of variability that the error bars are capturing should be clearly stated (for example, train/test split, initialization, random drawing of some parameter, or overall run with given experimental conditions).
   - The method for calculating the error bars should be explained (closed form formula, call to a library function, bootstrap, etc.)
   - The assumptions made should be given (e.g., Normally distributed errors).

- It should be clear whether the error bar is the standard deviation or the standard error of the mean.
- It is OK to report 1-sigma error bars, but one should state it. The authors should preferably report a 2-sigma error bar than state that they have a 96% CI, if the hypothesis of Normality of errors is not verified.
- For asymmetric distributions, the authors should be careful not to show in tables or figures symmetric error bars that would yield results that are out of range (e.g. negative error rates).
- If error bars are reported in tables or plots, The authors should explain in the text how they were calculated and reference the corresponding figures or tables in the text.

8. **Experiments Compute Resources**

   Question: For each experiment, does the paper provide sufficient information on the computer resources (type of compute workers, memory, time of execution) needed to reproduce the experiments?

   Answer: [Yes]

   Justification: We provided them in Section 4.1.

   Guidelines:

   - The answer NA means that the paper does not include experiments.
   - The paper should indicate the type of compute workers CPU or GPU, internal cluster, or cloud provider, including relevant memory and storage.
   - The paper should provide the amount of compute required for each of the individual experimental runs as well as estimate the total compute.
   - The paper should disclose whether the full research project required more compute than the experiments reported in the paper (e.g., preliminary or failed experiments that didn't make it into the paper).

9. **Code Of Ethics**

   Question: Does the research conducted in the paper conform, in every respect, with the NeurIPS Code of Ethics `https://neurips.cc/public/EthicsGuidelines`?

   Answer: [Yes]

   Justification: Our research conforms the Code of Ethics.

   Guidelines:

   - The answer NA means that the authors have not reviewed the NeurIPS Code of Ethics.
   - If the authors answer No, they should explain the special circumstances that require a deviation from the Code of Ethics.
   - The authors should make sure to preserve anonymity (e.g., if there is a special consideration due to laws or regulations in their jurisdiction).

10. **Broader Impacts**

    Question: Does the paper discuss both potential positive societal impacts and negative societal impacts of the work performed?

    Answer: [NA]

    Justification: Image denoising is a basic image processing task.

    Guidelines:

    - The answer NA means that there is no societal impact of the work performed.
    - If the authors answer NA or No, they should explain why their work has no societal impact or why the paper does not address societal impact.
    - Examples of negative societal impacts include potential malicious or unintended uses (e.g., disinformation, generating fake profiles, surveillance), fairness considerations (e.g., deployment of technologies that could make decisions that unfairly impact specific groups), privacy considerations, and security considerations.

- The conference expects that many papers will be foundational research and not tied to particular applications, let alone deployments. However, if there is a direct path to any negative applications, the authors should point it out. For example, it is legitimate to point out that an improvement in the quality of generative models could be used to generate deepfakes for disinformation. On the other hand, it is not needed to point out that a generic algorithm for optimizing neural networks could enable people to train models that generate Deepfakes faster.
- The authors should consider possible harms that could arise when the technology is being used as intended and functioning correctly, harms that could arise when the technology is being used as intended but gives incorrect results, and harms following from (intentional or unintentional) misuse of the technology.
- If there are negative societal impacts, the authors could also discuss possible mitigation strategies (e.g., gated release of models, providing defenses in addition to attacks, mechanisms for monitoring misuse, mechanisms to monitor how a system learns from feedback over time, improving the efficiency and accessibility of ML).

11. **Safeguards**

    Question: Does the paper describe safeguards that have been put in place for responsible release of data or models that have a high risk for misuse (e.g., pretrained language models, image generators, or scraped datasets)?

    Answer: [NA]

    Justification: Our paper poses no such risks.

    Guidelines:

    - The answer NA means that the paper poses no such risks.
    - Released models that have a high risk for misuse or dual-use should be released with necessary safeguards to allow for controlled use of the model, for example by requiring that users adhere to usage guidelines or restrictions to access the model or implementing safety filters.
    - Datasets that have been scraped from the Internet could pose safety risks. The authors should describe how they avoided releasing unsafe images.
    - We recognize that providing effective safeguards is challenging, and many papers do not require this, but we encourage authors to take this into account and make a best faith effort.

12. **Licenses for existing assets**

    Question: Are the creators or original owners of assets (e.g., code, data, models), used in the paper, properly credited and are the license and terms of use explicitly mentioned and properly respected?

    Answer: [Yes]

    Justification: We cited the paper that provided pre-trained diffusion models and we also included the corresponding URL.

    Guidelines:

    - The answer NA means that the paper does not use existing assets.
    - The authors should cite the original paper that produced the code package or dataset.
    - The authors should state which version of the asset is used and, if possible, include a URL.
    - The name of the license (e.g., CC-BY 4.0) should be included for each asset.
    - For scraped data from a particular source (e.g., website), the copyright and terms of service of that source should be provided.
    - If assets are released, the license, copyright information, and terms of use in the package should be provided. For popular datasets, `paperswithcode.com/datasets` has curated licenses for some datasets. Their licensing guide can help determine the license of a dataset.
    - For existing datasets that are re-packaged, both the original license and the license of the derived asset (if it has changed) should be provided.

- If this information is not available online, the authors are encouraged to reach out to the asset's creators.

13. **New Assets**

    Question: Are new assets introduced in the paper well documented and is the documentation provided alongside the assets?

    Answer: [NA]

    Justification: Our paper did not release new assets.

    Guidelines:

    - The answer NA means that the paper does not release new assets.
    - Researchers should communicate the details of the dataset/code/model as part of their submissions via structured templates. This includes details about training, license, limitations, etc.
    - The paper should discuss whether and how consent was obtained from people whose asset is used.
    - At submission time, remember to anonymize your assets (if applicable). You can either create an anonymized URL or include an anonymized zip file.

14. **Crowdsourcing and Research with Human Subjects**

    Question: For crowdsourcing experiments and research with human subjects, does the paper include the full text of instructions given to participants and screenshots, if applicable, as well as details about compensation (if any)?

    Answer: [NA]

    Justification: Our paper does not involve crowdsourcing nor research with human subjects

    Guidelines:

    - The answer NA means that the paper does not involve crowdsourcing nor research with human subjects.
    - Including this information in the supplemental material is fine, but if the main contribution of the paper involves human subjects, then as much detail as possible should be included in the main paper.
    - According to the NeurIPS Code of Ethics, workers involved in data collection, curation, or other labor should be paid at least the minimum wage in the country of the data collector.

15. **Institutional Review Board (IRB) Approvals or Equivalent for Research with Human Subjects**

    Question: Does the paper describe potential risks incurred by study participants, whether such risks were disclosed to the subjects, and whether Institutional Review Board (IRB) approvals (or an equivalent approval/review based on the requirements of your country or institution) were obtained?

    Answer: [NA]

    Justification: the paper does not involve crowdsourcing nor research with human subjects.

    Guidelines:

    - The answer NA means that the paper does not involve crowdsourcing nor research with human subjects.
    - Depending on the country in which research is conducted, IRB approval (or equivalent) may be required for any human subjects research. If you obtained IRB approval, you should clearly state this in the paper.
    - We recognize that the procedures for this may vary significantly between institutions and locations, and we expect authors to adhere to the NeurIPS Code of Ethics and the guidelines for their institution.
    - For initial submissions, do not include any information that would break anonymity (if applicable), such as the institution conducting the review.